2023-05-01

Analysis of the electrostatic characteristics of the Zika virus capsid using computational methods

Cassandra Guadalupe Del Rio De Avila
University of Texas at El Paso

ANALYSIS OF THE ELECTROSTATIC CHARACTERISTICS OF THE ZIKA VIRUS CAPSID USING COMPUTATIONAL METHODS

CASSANDRA GUADALUPE DEL RIO DE AVILA

Master's Program in Physics

APPROVED:

Lin Li, Ph.D., Chair

Jorge Munoz, Ph.D.

Jianjun Sun, Ph.D.

Stephen L. Crites, Jr., Ph.D.
Dean of the Graduate School

To me,

as a reminder of the hard beginnings, exhausting processes, and pleasing endings

ANALYSIS OF THE ELECTROSTATIC CHARACTERISTICS OF THE ZIKA VIRUS CAPSID USING COMPUTATIONAL METHODS

by

CASSANDRA GUADALUPE DEL RIO DE AVILA, B.S.

THESIS

Presented to the Faculty of the Graduate School of

The University of Texas at El Paso

in Partial Fulfillment

of the Requirements

for the Degree of

MASTER OF SCIENCE

Department of Physics

THE UNIVERSITY OF TEXAS AT EL PASO

May 2023

Acknowledgments

I would like to express my gratitude to Dr. Lin Li, my advisor, and Assistant Professor of the Physical Science Department, for his valuable support, patience, and guidance during my time in his research group. Similarly, I would like to thank my lab mates, Wenhan, Shengjie, Jason, and Alan, for their help and patience in teaching me. Their hard work and dedication are an inspiration to me, and I am grateful for everything they have taught me. Their assistance was essential in making this work possible. Furthermore, I want to acknowledge Dr. Jorge Munoz and Dr. Jianjun Sun, my committee members, for their valuable time and consideration in reading and reviewing my work.

I am deeply grateful for the love, support, and motivation of my family. Obtaining my master's degree at UTEP is the result of their unconditional support and encouragement, which has motivated me every day to never give up and pursue my goals. To Lenin, who has been my unconditional friend above all and who has been by my side despite the distance, I thank you for sharing your time with me and letting me share mine with you. I thank my friends, Valeria, Sara, Joy, Bianca, Fidel, Vanessa, Daniela, and the rest of my friends in El Paso, for their advice and for sharing pleasant and fun moments with me.

Abstract

Zika virus (ZIKV) is a flavivirus that is usually transmitted through the bite of infected mosquitoes. This virus can cause a variety of neurological disorders, the most common being Guillain-Barré syndrome in adults. Moreover, it is of great concern in pregnant women, since can cause deformities in the brain and other organs of newborns.

Studying the structural characteristics of the virus during its mature and infectious phase can provide crucial information on the mechanisms by which it enters and replicates within host cells, as well as its evolution, transmission, and interaction with other living organisms.

The symmetric pattern present in the virus capsid allowed the identification of four binding modes in the Zika virus capsid, each consisting of two heterotetramers formed from two copies of the E protein and two M proteins. In addition, several computational methods were used to calculate the electrostatic properties and understand the interactions between the heterotetramers that make up the binding modes present in the Zika virus capsid. That is why the study of the structural characterization and conformational changes of the envelope protein (E) is crucial to understand the binding and fusion of the virus with the host cell membrane.

The findings of this study may aid in future drug design against the Zika virus by providing valuable information on the structural properties and interactions between E proteins during different stages of infection.

Table of Contents

List of Figures

List of Illustrations

Chapter 1: Introduction

1.1 Motivation

Studying the electrostatic features of the Zika virus' capsid assembly can provide important insights into the mechanism of virus assembly and its interactions with host cells. Electrostatic interactions are known to play a crucial role in the assembly of viruses, including the Zika virus, by facilitating the formation of protein-protein and protein-RNA complexes. By understanding the electrostatic interactions that govern the Zika virus capsid assembly, we can identify potential targets for antiviral drugs and develop new strategies for preventing and treating Zika virus infections. Moreover, the study of electrostatic features can also help us to understand the role of viral proteins in triggering host immune responses and provide insights into the design of new vaccines against Zika virus.

1.2 Zika Virus

Zika virus is a member of the flavivirus genus, which is a subgroup of the Flaviviridae family. Other viruses in this genus include Dengue virus (DENV), Yellow fever virus (YFV), West Nile virus (WNV), and Japanese encephalitis virus (JEV). These viruses share many common characteristics, such as their genetic makeup, structure, and mode of transmission [1,2].

These flaviviruses are primarily transmitted to humans by arthropod vectors, which are typically mosquitoes or ticks. In the case of the Zika virus, the primary vector is the Aedes mosquito. Because ZIKV is primarily transmitted by mosquitoes, it is known as a mosquito-borne viral disease. This means that the virus is transmitted to humans through the bite of an infected mosquito [3,4].

1.2.1 Historical Background

Zika virus was first identified in monkeys in the Zika forest in 1947. Eventually, the virus was spread by Aedes mosquitoes until it was first identified in humans in the 1950s. Although Aedes mosquitoes are considered the main Zika virus vector, alternative means of transmission include from mother to fetus during pregnancy, spread through sexual contact, breastfeeding, blood transfusion, and possibly through organ transplantation [4-6]. The majority of Zika virus infections are likely asymptomatic when a symptomatic disease occurs it is characterized by a subclinical or mild illness similar to influenza [5]. The most reported symptoms of Zika include red eyes, headache, fever, rash, muscle pain, joint pain, fatigue, and conjunctivitis [2,7].

The Zika virus outbreak in French Polynesia in 2013 was followed by an increase in adult cases of Guillain Barré syndrome and associated neurological conditions. In addition, in the months after the Zika virus epidemic in Brazil in 2015, there was a sharp rise in the number of infants born with congenital microcephaly. This led the World Health Organization to declare an international public health emergency in 2016 [4-9].

At present, there is no specific antiviral treatment available for Zika virus infection, so only supportive care is provided. This includes using medications like analgesics (pain relievers) and antipyretics (fever reducers), as well as fluids and rest, to manage the symptoms and keep the patient comfortable [5].

The Aedes mosquito is the target of most control methods for the Zika virus. This is because the virus is primarily transmitted to humans through the bite of infected Aedes mosquitoes. Therefore, the main preventive measure is to avoid being bitten by mosquitoes in areas where ZIKV is present. This can be done by using insect repellents, wearing long-sleeved clothing, and staying in places with air conditioning or screened windows and doors [4].

While the number of reported Zika virus cases has decreased since the most recent outbreaks in the Americas, Asia, and Africa, treatment of the virus is still urgent. This is because there is currently no vaccine or specific treatment for Zika virus infection, and it can cause serious health problems in certain populations, such as pregnant women and their fetuses. Therefore, it is important to continue efforts to prevent the spread of the Zika virus and manage its symptoms until a more effective treatment or vaccine becomes available. [10,11]

1.2.2 Biological Structure

Studying the structural characteristics of a virus in its mature and infectious stage, such as its shape, size, and composition, can help to understand how it evolved, how it spreads, and how it interacts with other organisms. In this way, it is possible to gain valuable insights into the mechanisms by which the virus enters host cells and replicates inside them. This knowledge is essential for developing effective treatments, such as antiviral drugs and vaccines, that can target specific aspects of the virus's life cycle.

Moreover, by identifying the virus's weak points or vulnerable spots, such as regions on its outer shell or envelope that are critical for its interaction with host cells, scientists can develop novel strategies to combat the virus. For example, if scientists can design drugs or vaccines that specifically target these vulnerable spots, they can potentially prevent the virus from infecting host cells or reduce the severity of the disease it causes.

ZIKV is a virus that has an envelope. The envelope is made up of three structural proteins called capsid (C), membrane (M), and envelope (E) glycoprotein. The virus's genetic material, RNA, is surrounded by multiple copies of the C protein and is enclosed by the E and M proteins. All of this is anchored in a lipid membrane. The surface of the virus is decorated with the E and

M proteins arranged on an icosahedral surface. This arrangement is found in other viruses from the Flaviviridae family, to which ZIKV belongs [2, 12].

The mature structure of ZIKV consists of 180 copies of the E protein (90 E-dimer) and 180 copies of the M protein (90 M-dimer), which, in turn, form 90 E:M heterodimers [13].

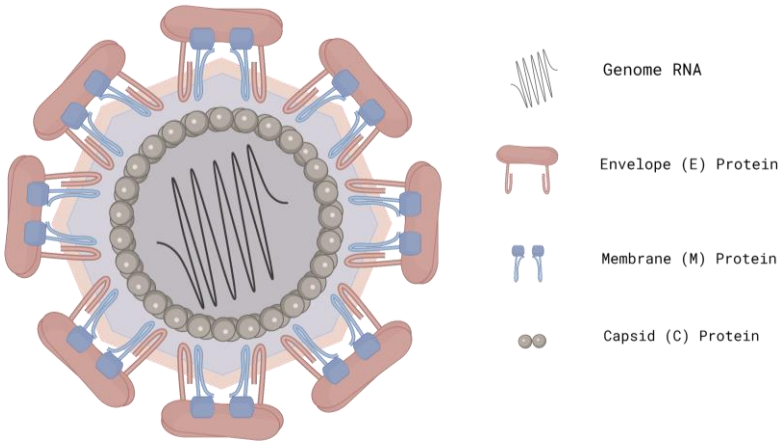

Illustration 1.1. Schematic representation of the Zika virus virion. ZIKV counts with an envelope made of three proteins: Capsid (C), Membrane (M), and Envelope (E). The nucleocapsid contains the RNA genome and is bound to the C protein. The surface or capsid of the virion has an icosahedral symmetry, where the E and M proteins are located.

The E protein is a surface protein that is crucial for the binding and fusion of the virus with the host cell's membrane. One of the functions of the E protein is to target specific receptors on the surface of the host cell. Once the virus has attached to the cell, the E protein then plays a critical role in the fusion process. It is responsible for fusing the virus and the host cell membranes together, which allows the virus to enter the host cell [14].

Mosquitoes transmit ZIKV to humans by injecting the virus into the skin during blood feeding. The virus infects permissive cells, including skin cells in the epidermis and dermis, which are the first line of defense. The virus uses multiple receptors to enter host cells through the

envelope protein, which interacts with cell surface receptors [2,15,16]. Flaviviruses exist in three states during their life cycle: immature, mature, and fusogenic which are noninfectious, infectious, and host membrane–binding states, respectively [13]. The maturation state of flaviviruses can have significant biological implications, such as influencing the effects of antibody binding [12].

Chapter 2: Methods

2.1 Structure Preparation

The mature structure of the Zika virus was obtained from the Protein Data Bank (PDB) and determined by cryo-electron microscopy (cryo-EM), at a near-atomic resolution of 3.8 angstroms.

Chimera software was employed to observe the full capsid structure [17]. As shown in Figure 2.1, the capsid assembly (made of the E:M heterodimers) has a symmetric arrangement, which allowed us to identify four different binding modes that represent all possible interactions between heterodimers [18].

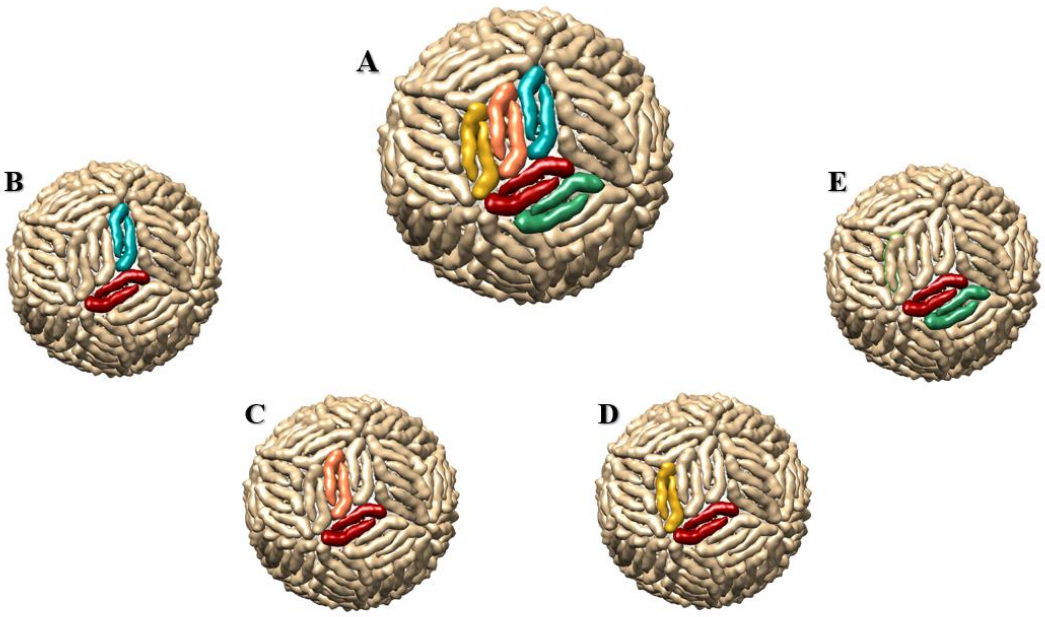

Figure 2.1. Capsid structure of the Zika virus. (A)The full structure consists of five heterotetramers, which are represented by four different binding modes. (B) Binding mode I is composed of two heterodimers colored in cyan and red, arranged perpendicular to each other. (C) Binding mode II is composed of two heterodimers colored in orange and red, also arranged perpendicular to each other. (D) Binding mode III is composed of two heterodimers colored in yellow and red, also arranged perpendicular to each other. (E) Binding mode IV is composed of two heterodimers arranged parallel to each other, and this binding mode can be represented by using, for example, the heterodimers orange and yellow.

Although the M protein is a structural protein that helps in assembling and releasing viruses from infected cells, in this study it does not play a significant role in the assembly of the capsid, particularly the binding of E proteins. As a result, the M protein was excluded from the simulations and focused only on studying the assembly of the capsid through the E protein.

The data used in the study only include the E protein, and Figure 2.2 illustrates a visual representation of the E proteins and their binding in the assembly process.

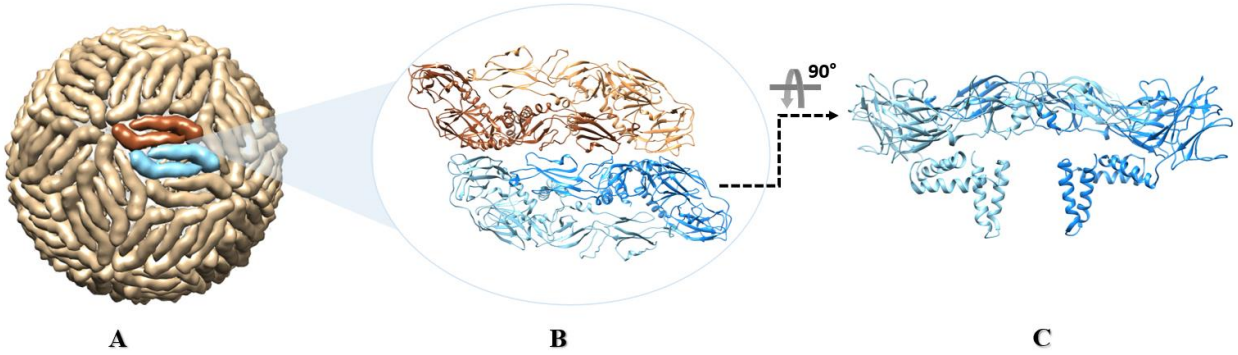

Figure 2.2. Binding assembly of complex units of the Zika virus capsid. (A) Structure of the Zika virus capsid and identification of binding modes made of two complex units colored in blue and brown. (B) Two Binding units in a ribbon form. (C) Side view of one of the heterodimers composed by two copies of E protein.

2.2 Electrostatic Calculations

To study the electrostatic properties of the Zika virus capsid, DelPhi [19] and DelPhiForce [20] are software tools that are widely used to calculate and visualize the electrostatic properties of biomolecules with high accuracy. In the case of the E-monomer and each binding domain, these tools were employed to analyze the electrostatic potential and overall force in order to gain insights into their structural and functional characteristics.

2.2.1 DelPhi Calculations

DelPhi was used to calculate the electrostatic potential at the surface of each unit that makes up the different binding modes. This allowed analyzing how electrostatic forces might be involved in the formation of the capsid and its interactions with other molecules.

DelPhi is a software program that uses a method called continuum electrostatics to calculate the electrostatic potential in complex biological systems that contain macromolecules and water in presence of mobile ions. This potential is a measure of the attractive or repulsive forces between charged particles in the system [18].

To calculate this potential, DelPhi solves a mathematical equation called the Poisson-Boltzmann equation (PBE):

$$[\nabla \cdot \epsilon(r)\nabla\phi(r)] = -4\pi\rho(r) + \epsilon(r)k^2(r)\sinh(\phi(r)/k_bT) \qquad (2.1)$$

Where $\phi(r)$ is the electrostatic potential $\epsilon(r)$ is the dielectric distribution $\rho(r)$ is the charge density based on the atomic structures, k is the Debye-Huckel parameter, k_b is the Boltzmann constant, and T is the Temperature. Due to the irregular shape of macromolecules, DelPhi uses a finite difference (FD) to solve the PBE.

The Poisson-Boltzmann equation is a mathematical equation that describes how charged particles interact with each other in a solution, considering the effects of the solvent and the ions in the solution. In the context of biological macromolecules, the PBE can be used to calculate the distribution of electrostatic potential and ion concentrations around the molecule, which can in turn provide information about its stability, binding, and other properties [21].

The DelPhi program implements the Poisson-Boltzmann equation to calculate electrostatic interactions in biological macromolecules. It does this by discretizing the molecule into a grid of points and then solving the Poisson-Boltzmann equation at each point to obtain the electrostatic

potential. The program can handle various types of boundary conditions, such as a fixed charge or a charged surface, and can also perform calculations for multiple conformations of the molecule[19].

To perform DelPhi calculations, PQR and Gaussian cube files were generated for each E protein monomer and E-dimer using PDB2PQR [22]. These files were then visualized using Chimera. In the visualization, a color scale ranging from -1.0 $kT/$Å to 1.0 $kT/$Å was used.

The electrostatic potential map generated by DelPhi calculations was used as the basis for implementing Visual Molecular Dynamics (VMD) [23] to visualize the electric field lines between the heterodimers comprising the four different binding modes. To enhance the visualization of these electric field lines using VMD, the distance between the selected heterodimers was extended by 20 Å, utilizing the center of mass of the heterodimers as a point of reference.

2.2.2 DelPhiForce Calculations

To calculate the forces involved in interactions between heterodimers DelPhiForce tool [20] was implemented. To gain a deeper understanding of the interactions between the charged particles involved in the binding process, each one of the four binding modes was modified to obtain different configurations or arrangements. Through this approach, we were able to observe how the charged particles interact with each other and how they are bound together.

To generate modified configurations for each binding mode, we used the structureMan software [24] to displace the blue, orange, yellow, and green heterodimers with respect to the fixed red heterodimer (Figure 2.1), within a range of 8A to 40A in 2A intervals. In total, 12 modified configurations were generated for each binding mode. The electrostatic binding forces between

the molecules were then calculated using DelPhiForce, and these forces were visualized in VMD as blue arrows.

Chapter 3: Results & Discussion

3.1 Electrostatic Potential Surface

The present study investigated the electrostatic characteristics of the five heterodimers composing different binding modes in the Zika virus capsid. The first feature analyzed was the electrostatic potential, which was calculated using DelPhi to determine the electrostatic surface. The charge distribution on the Zika virus E protein was then visualized using Chimera, with a color scale ranging from -1.0 to 1.0 kT/e. The color scheme consisted of blue, red, and white-colored areas that corresponded to positively, negatively, and neutrally charged potentials, respectively. Notably, the predominant charge in all five heterodimers was positive (blue-colored areas), while negative and neutral charges were scattered on the surface. This observation was consistent across all binding modes, indicating a similar electrostatic potential among them. Therefore, the electrostatic potential of the Zika virus E protein and its heterodimers appears to be an important factor to consider in the Zika capsid binding mechanism.

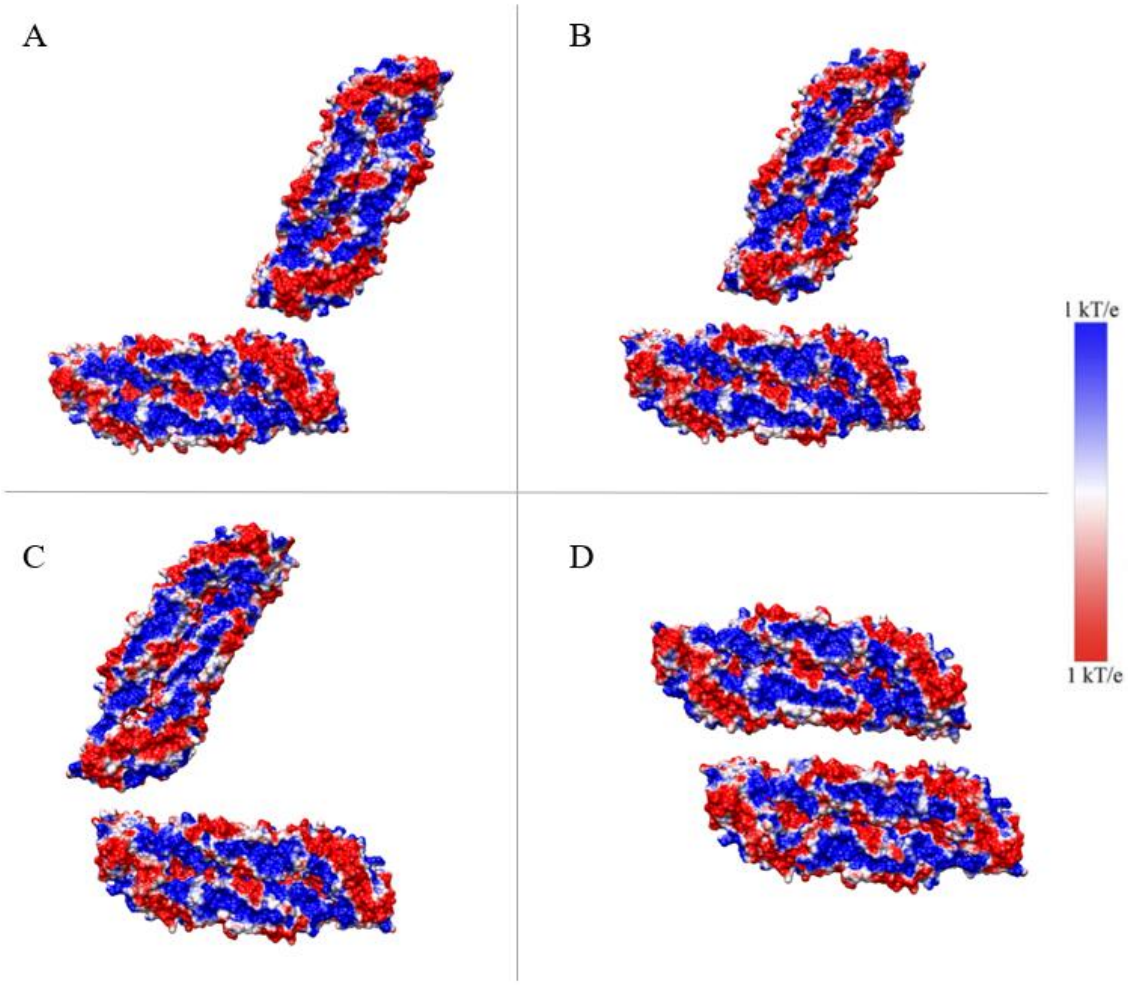

Figure 3.1: Electrostatic potential surfaces of binding modes. Panels (A), (B), (C), and (D) show the electrostatic surfaces of binding modes I, II, III, and IV, respectively, visualized in Chimera with a color scale ranging from -1.0 to 1.0 kT/e. The color scheme utilized blue, red, and white colored areas to represent positively, negatively, and neutrally charged potentials, respectively.

The electrostatic potential surfaces provide a clear and concise visual representation of the charge distribution on the E-dimer surfaces found in the Zika virus capsid. This observed charge distribution plays a fundamental role in explaining the binding and interaction between these heterodimers or proteins.

Figure 3.2 (A) illustrates the complex unit of binding mode IV, consisting of two E-dimer complex units colored red and green, along with the corresponding electrostatic potential surface at the bottom. To view the interface of each E protein dimer, the visualization angle was rotated 90° as shown in Figure 3.2 (B). Figure 3.2 (C) shows the red complex unit and its electrostatic surface, with the primary binding sites marked by yellow and green circles. The charge distribution at the binding sites was observed individually for each heterodimer, with the same process carried out for the green complex unit. Upon rotating the view 180 degrees, a similar charge distribution was seen at the contact, as shown in Figure 3.2 (D).

When the two heterodimers are bind (as shown in Figure 3.2 A), - the charge distribution in the green circles complement each other - the same happens with the charge distribution within the yellow circles, resulting in a stable binding mode and providing a more detailed understanding of the binding mechanism [25,26].

The information gained from these surfaces can be utilized to understand molecular interactions. These electrostatic potential surfaces constitute an important contribution to the field of Zika virus research and provide valuable insights into the mechanisms of viral entry and pathogenicity.

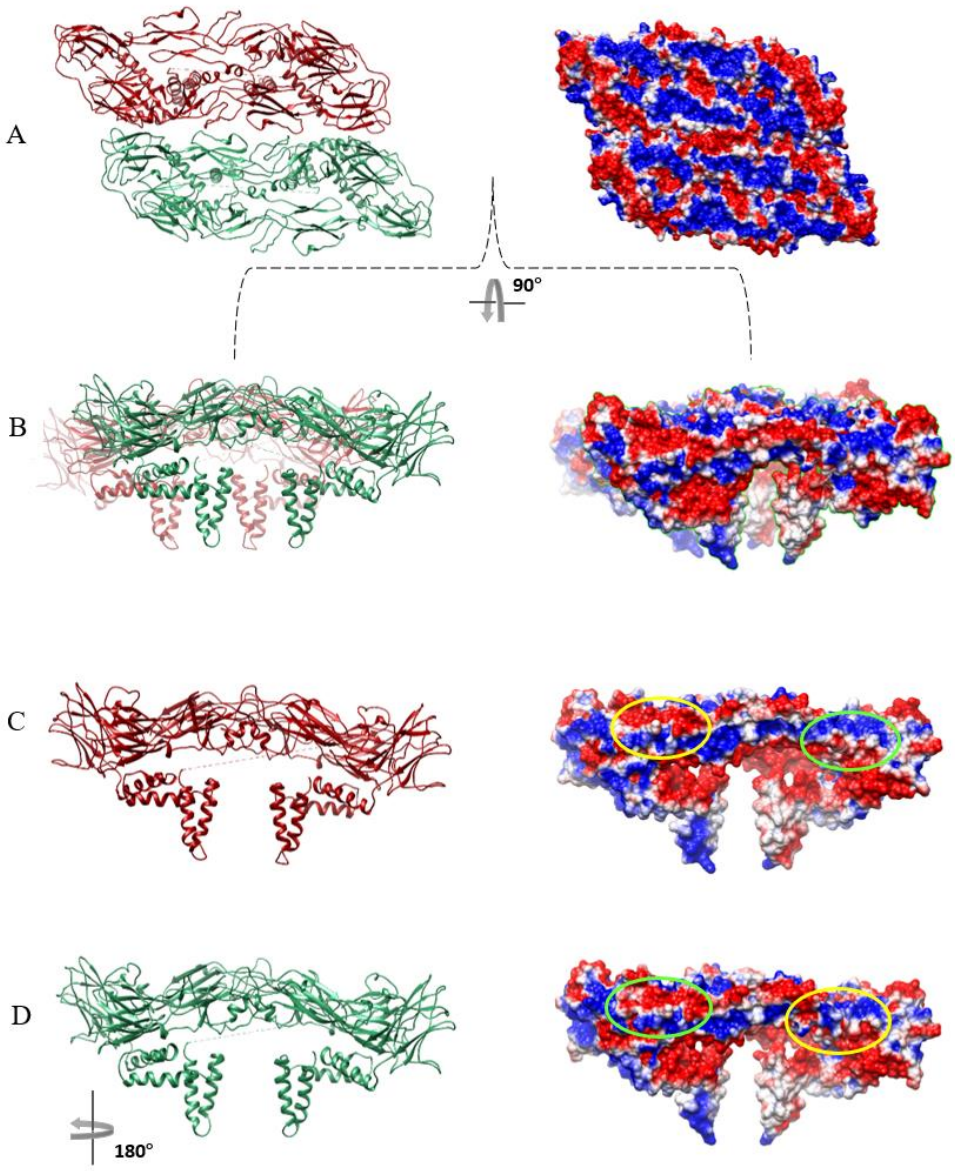

Figure 3.2. Electrostatic potential surface and charge distribution for binding mode IV. The charge distribution of binding mode IV was used as an example to better understand how proteins bind. Figures (A) and (B) show the complex structure and potential surface for binding mode IV. Figure (B) shows a view rotated 90 degrees. Figure (C) shows a side view of the complex structure and charge distribution of the heterodimer colored in red. On the other hand, Figure (D) shows a side view of the complex structure and the charge distribution for the heterodimer colored in green; this is a view rotated 180 degrees. The areas within the green ovals are in contact with each other, while the areas within the yellow ovals are in contact with each other.

3.2 Electrostatic Field Lines

Using Delphi calculation data and Visual Molecular Dynamics (VMD), we generated a visualization of the electrostatic field lines for each binding mode. While the electrostatic surface displays a similar charge distribution across different heterodimers, the density of field lines is expected to vary for each binding mode due to the distribution of charges in the contact area between the heterodimers.

To obtain a better visualization of the electrostatic field lines, each binding mode was modified by fixing the heterodimer colored in red (Figure 2.2) and shifting the remaining heterodimers 20Å from the fixed heterodimer. This adjustment allowed us to observe a significant difference in the number of field lines for each binding mode. However, there were still noticeable differences when the interface areas were examined more closely.

Binding mode IV had the largest interaction due to the larger contact area between the heterodimers, which leads to a greater number of electrostatic field lines. On the other hand, in modes I, II, and III, where the heterodimers are positioned perpendicular to one another, a similar density of field lines is observed at first glance, but on closer examination, differences in the number of lines are apparent, as shown in Figure 3.3. To obtain more precise information on the differences in the interaction between the heterodimers in these binding modes, a more detailed study is required. In the next section, a feature that may help to achieve this will be described.

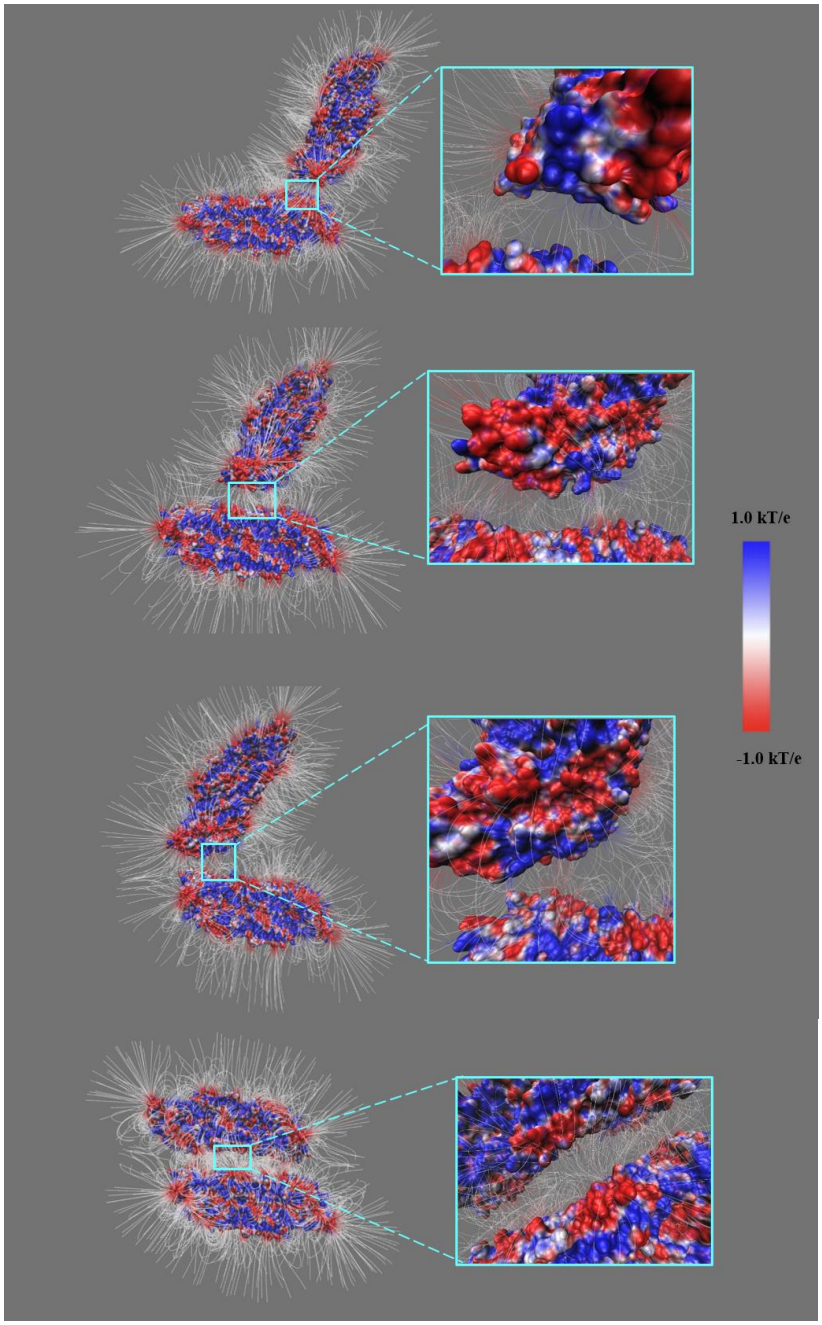

Figure 3.3. Figure 3.3. Electrostatic field lines at the heterodimers' interfaces form the 4 binding modes. An overview of electric field lines for binding modes I, II, III, and IV is shown on the left side of panels (A), (B), (C), and (D) respectively. A close-up view of heterodimers' interfaces is shown on the right side of these panels. Visual Molecular Dynamics (VMD) renders the electrostatic surfaces and field lines with a color scale from -1.0 to 1.0 kT/Å.

3.3 Electrostatic Forces

The electrostatic force exerted between the heterodimers that make up the four different binding modes was calculated using DelPhiForce. From each binding mode, 17 different configurations were obtained, where the distance between the heterodimers ranged from 8 angstroms to 40 angstroms, in intervals of 2 angstroms. The electrostatic force for each configuration is represented with blue arrows, as shown in Figure 3.4. To better visualize the net force between proteins, the magnitude of the forces is normalized so that they are of the same scale at different distances. This means that the length of the arrows does not represent the magnitude of the force, they only represent the direction of the forces [27].

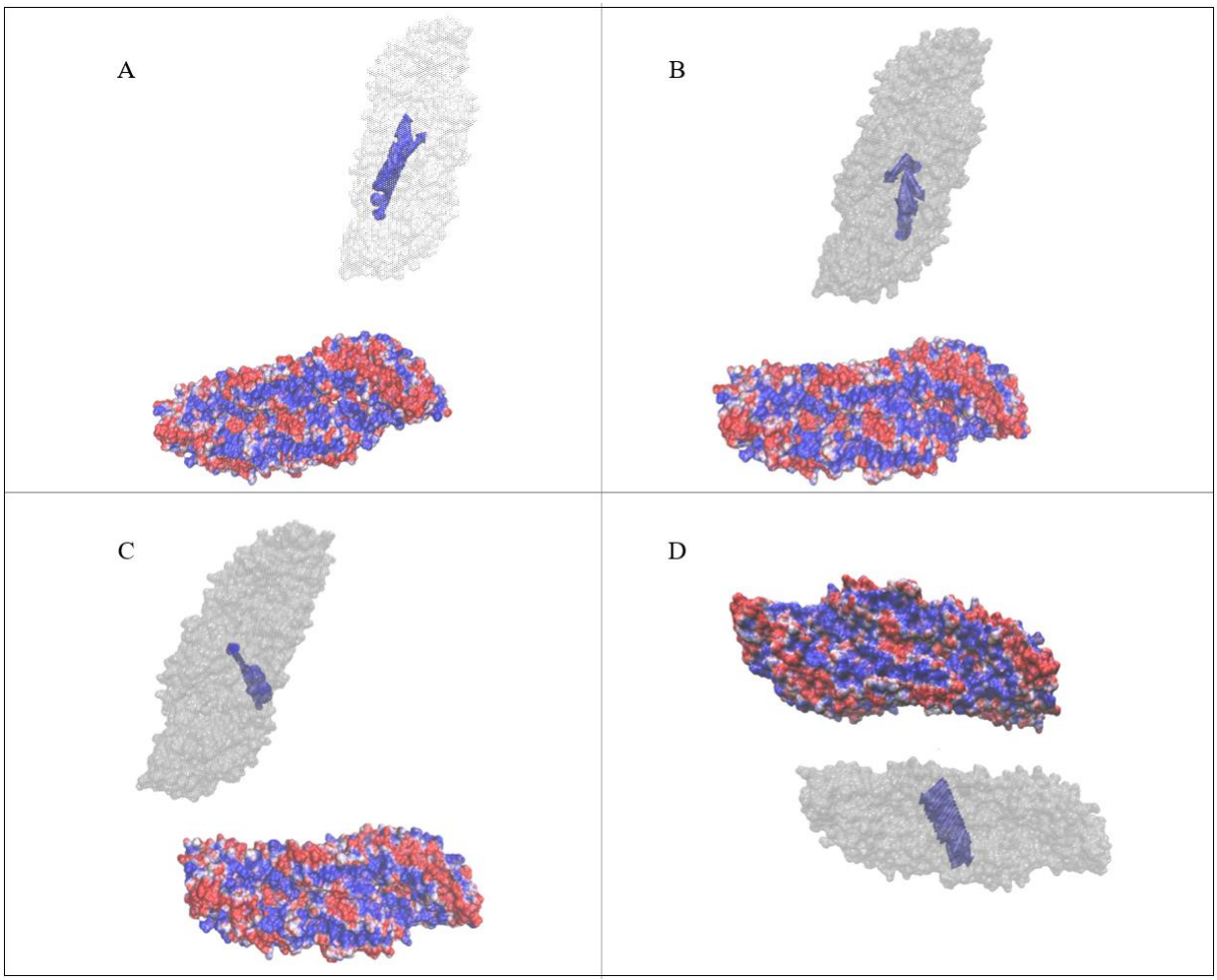

Figure 3.4. The electrostatic net force between heterodimers in all four binding modes. The electrostatic net force between heterodimers in all four binding modes is represented by blue arrows at different distances. VMD was used to render all modes, and the fixed heterodimer is shown in all panels with its electrostatic surface. Red and blue colors represent negatively and positively charged areas, respectively, with a color scale ranging from -1.0 to 1.0 kT/a. The manipulated heterodimer surfaces are depicted in light grey. Panels A and D (binding modes I and IV, respectively) exhibit a repulsive net force, with mode IV being stronger. Panels B and C (binding modes II and III, respectively) display an attractive net force, with mode II being stronger.

Figure 3.4A shows an overall repulsive force between the red and blue heterodimers (Figure 2.2). A more detailed analysis is presented in Figure 3.5A, where the direction of the blue arrows representing the net electrostatic force is shown in greater detail. In this figure, we can observe how the direction of the arrows change at different separation distances.

In addition, in Figures 3.5B and 3.5C, red arrows representing the electrostatic force for individual residues at 8 Å of distance can also be seen. These arrows represent both the direction and magnitude of the force. Figure 3.4B depicts an overall attractive force between the red and orange heterodimers (Figure 2.2). Figure 3.5D provides a more detailed view of the direction of the arrows. In this binding mode, the arrows do not change their direction significantly as the separation distance increases, unlike the previous binding mode. Additionally, the red arrows representing the electrostatic force for individual residues at 8 Å of distance can also be seen in Figures 3.5E and 3.5F. Figure 3.4C shows a general attractive force between the red and yellow heterodimers (Figure 2.2). Figure 3.6A provides a more detailed view of the direction of the arrows. This binding mode exhibits a weaker attractive force than the previous one. Also, the red arrows representing the electrostatic force for individual residues at 8 Å of distance can also be seen in Figures 3.6B and 3.6C. Figure 3.4D shows a general repulsive force between the red and

green heterodimers (Figure 2.2). Figure 3.6D provides a more detailed view of the direction of the arrows. The direction of the blue arrows for this binding mode shows a stronger repulsive force than in binding mode I. Additionally, the red arrows representing the electrostatic force for individual residues at 8 Å of distance can also be seen in Figures 3.6E and 3.6F.

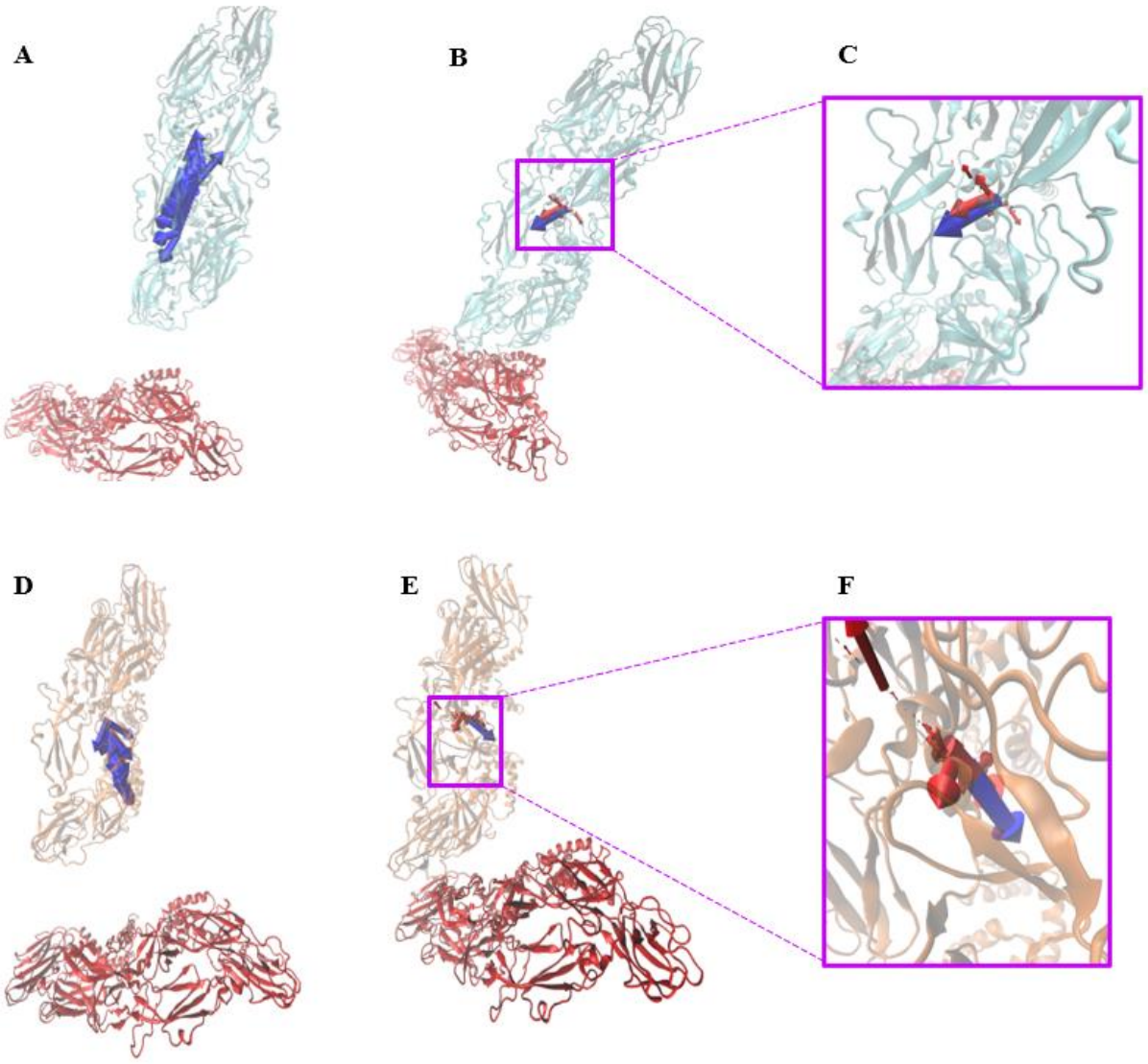

Figure 3.5. Electrostatic forces of Binding mode I and Binding mode II. (A) Shows the electrostatic forces of Binding Mode I at various distances ranging from 8 Å to 40 Å, with blue arrows indicating the direction of the net force. (B) Depicts the electrostatic force of Binding Mode I at 8 Å, where the blue arrow represents the total net force between the heterodimers colored in red and cyan, and red arrows denote individual forces between single residues. (C) Provides a close-up view of (B). (D) Shows the electrostatic forces of Binding Mode II at various distances ranging from 8 Å to 40 Å, with blue arrows indicating the direction of the net force. (E) Shows the electrostatic forces of Binding Mode II at 8 Å, where the blue arrow represents the total net force between the heterodimers colored in red and orange, and red arrows denote individual forces between single residues. (F) Provides a close-up view of (E).

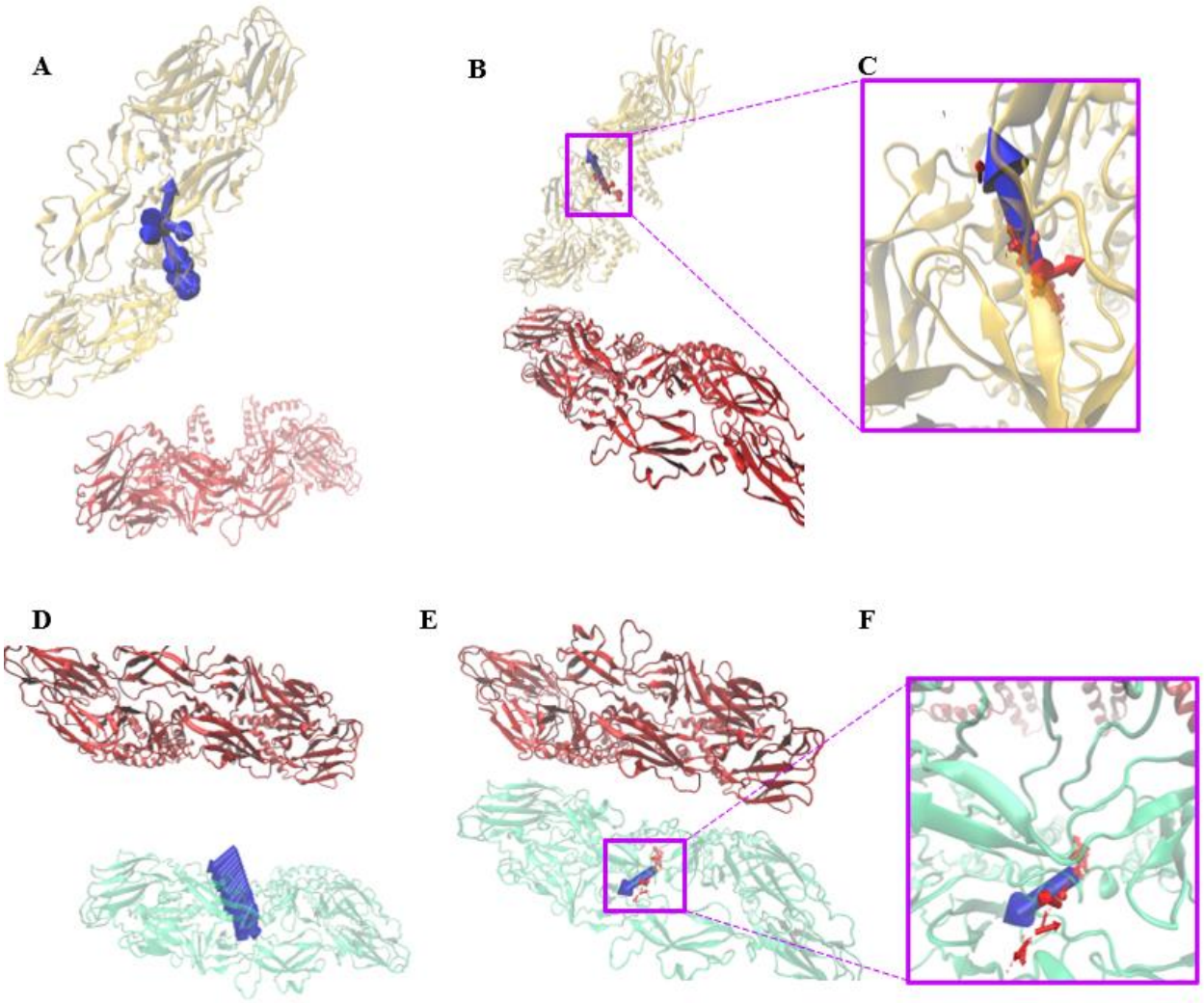

Figure 3.6. Electrostatic forces of Binding mode III and Binding mode IV. (A) Shows the electrostatic forces of Binding Mode III at various distances ranging from 8 Å to 40 Å, with blue arrows indicating the direction of the net force. (B) Depicts the electrostatic force of Binding Mode I at 8 Å, where the blue arrow represents the total net force between the heterodimers colored in red and yellow, and red arrows denote individual forces between single residues. (C) Provides a close-up view of (B). (D) Shows the electrostatic forces of Binding Mode IV at various distances ranging from 8 Å to 40 Å, with blue arrows indicating the direction of the net force. (E) Shows the electrostatic forces of Binding Mode IV at 8 Å, where the blue arrow represents the total net force between the heterodimers colored in red and green, and red arrows denote individual forces between single residues. (F) Provides a close-up view of (E).

Figure 3.7 depicts the magnitudes of net forces at varying distances. As illustrated in the figure, the attractive force between the heterodimers decreases as the distance between them increases, which is to be expected due to Coulomb's law.

In the study, the results for the net electrostatic force of four different binding modes were compared. It was observed that the strongest net force occurred between the heterodimers forming binding mode IV. The arrows in Figures 3.4 A and 3.5 A, however, show that this force is repulsive, contrary to expectations. On the other hand, the weakest net electrostatic force was produced between the heterodimers forming binding mode III, and it was an attractive force, as shown in the same figures. The charge distribution on the surface, the charge on the residues, as well as the contact area between heterodimers, are all contributing factors to these results.

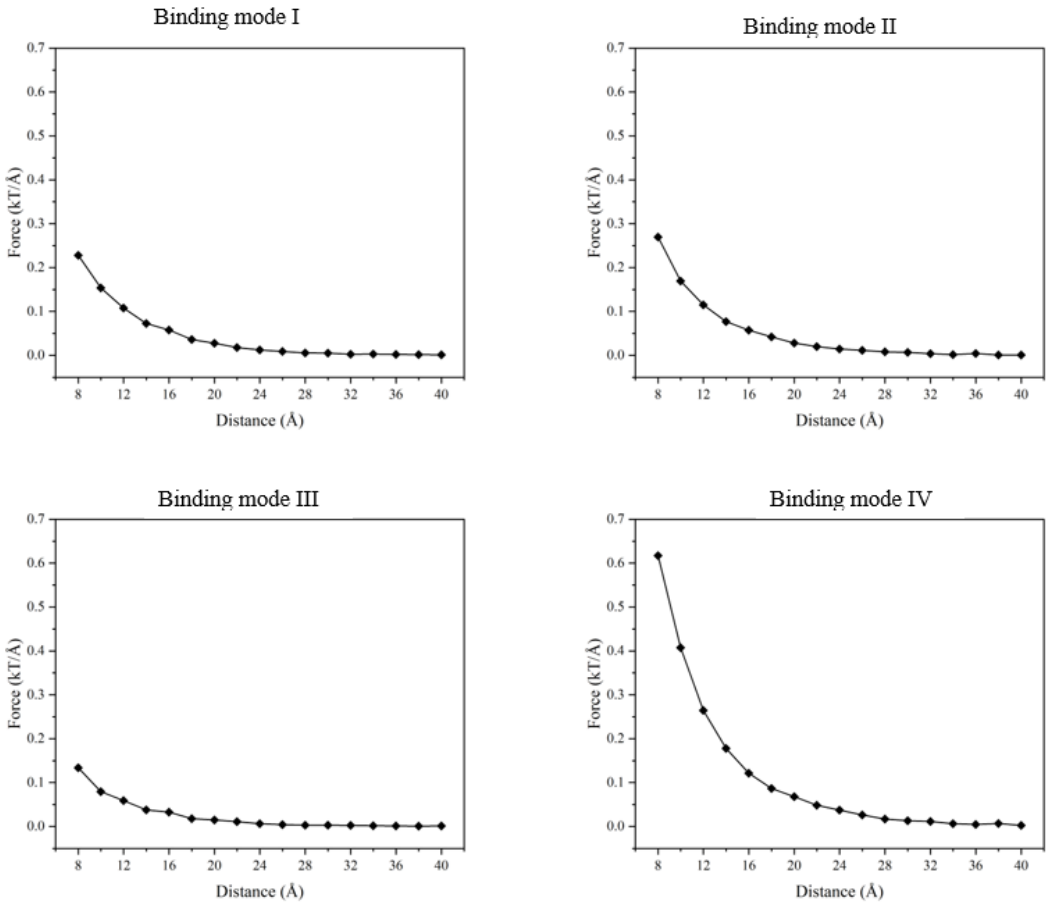

Figure 3.7. The net electrostatic force of each bonding mode as a function of distance. (A)Bonding mode 1 has a net repulsive force. (B) Bonding mode II shows an attractive force. (C) Binding mode III has the weakest net force among all binding modes. (D) Binding mode 4 has the highest net force interaction, but this is a repulsive force. The attractive force between the heterodimers decreases as the distance between them increases, which is expected due to Coulomb's law.

3.4 Future Work

As a continuation of this work, we intend to simulate dynamic protein-protein interactions. To identify key residues in electrostatic binding interactions, a salt bridge analysis can be performed [28,29] and analyzed following the molecular dynamics simulations by NAMD [30]. It is important to note that the simulation will focus on studying interactions between heterodimers,

which are proteins formed by two different subunits and will look for salt bridges found at the binding interface, i.e., in the area where both subunits join. To compare the results obtained in the different simulations, the formation of salt bridges in each binding mode will be analyzed. It is expected that the results of this comparison will be consistent with those obtained so far and will allow the identification of the key regions of the proteins involved in the electrostatic binding interactions.

Chapter 4: Conclusion

In this work, the electrostatic features of Zika virus capsid assembly were studied to better understand the mechanism of virus assembly, interactions with host cells, and potential antiviral drug targets. The mature structure was obtained by cryo-electron microscopy with an atomic resolution of 3.8. From the visualized structure, it was possible to identify four binding modes between the heterodimers forming the capsid assembly. The capsid structure was found to have a symmetric arrangement, and each binding mode consisted of two heterodimers arranged in specific orientations.

DelPhi was used to visualize the electrostatic potential and charge distribution on the surfaces of five Zika virus capsid heterodimers. The results showed that the electrostatic potential of the Zika virus E protein and its heterodimers could be an important consideration for potential drug development. In addition, the study used DelPhiForce to calculate the electrostatic force exerted between the heterodimers in the four different binding modes. The results showed that the strongest net force occurred in binding mode IV but was repulsive, contrary to expectations, and the weakest net electrostatic force occurred in binding mode III and was an attractive force. The charge distribution on the surface, the charge on the residues, and the contact area between the heterodimers were contributing factors to these results. This study demonstrates the key role of electrostatic forces in protein-protein interactions and provides valuable insights into the mechanisms of viral entry and pathogenicity for the Zika virus.

References

1. Haddow AD, Schuh AJ, Yasuda CY, Kasper MR, Heang V, et al. (2012) Genetic Characterization of Zika Virus Strains: Geographic Expansion of the Asian Lineage. PLoS Negl Trop Dis 6(2): e1477. doi: 10.1371/journal.pntd.0001477
2. Ávila-Pérez, G.; Nogales, A.; Martín, V.; Almazán, F.; Martínez-Sobrido, L. Reverse Genetic Approaches for the Generation of Recombinant Zika Virus. Viruses 2018, 10, 597. https://doi.org/10.3390/v10110597
3. Best, S. M. (2016). Flaviviruses. Current Biology, 26(24), R1258-R1260.
4. Benelli, G., & Romano, D. (2017). Mosquito vectors of Zika virus. Entomologia Generalis, 36(4), 309–318. doi:10.1127/entomologia/2017/0496.
5. Plourde AR, Bloch EM. A Literature Review of Zika Virus. Emerg Infect Dis. 2016 Jul;22(7):1185-92. doi: 10.3201/eid2207.151990. Epub 2016 Jul 15. PMID: 27070380; PMCID: PMC4918175.
6. Fauci, A. S., & Morens, D. M. (2016). Zika virus in the Americas—yet another arbovirus threat. New England journal of medicine, 374(7), 601-604.
7. World Health Organization (December 08, 2022). Zika virus. World Health Organization. https://www.who.int/news-room/fact-sheets/detail/zika-virus#:~:text=Key%20facts,last%20for%202%E2%80%937%20days.
8. Martines, R. B. (2016). Notes from the field: evidence of Zika virus infection in brain and placental tissues from two congenitally infected newborns and two fetal losses—Brazil, 2015. MMWR. Morbidity and mortality weekly report, 65.

9. European Centre for Disease Prevention and Control. Rapid risk assessment. Zika virus epidemic in the Americas: potential association with microcephaly and Guillain-Barré syndrome. 2015 Dec10. [cited 2016 Feb 3]. http://ecdc.europa.eu/en/publications/Publications/zika-virus-americasassociation-with-microcephaly-rapid-risk-assessment.pdf

10. Barouch, D. H., Thomas, S. J., & Michael, N. L. (2017). Prospects for a Zika virus vaccine. Immunity, 46(2), 176-182.

11. Larocca, R. A., Abbink, P., Peron, J. P. S., de A. Zanotto, P. M., Iampietro, M. J., Badamchi-Zadeh, A., ... & Barouch, D. H. (2016). Vaccine protection against Zika virus from Brazil. Nature, 536(7617), 474-478.

12. Heinz, F. X., & Stiasny, K. (2017). The antigenic structure of Zika virus and its relation to other flaviviruses: implications for infection and immunoprophylaxis. Microbiology and Molecular Biology Reviews, 81(1), e00055-16.

13. Sirohi, D., Chen, Z., Sun, L., Klose, T., Pierson, T. C., Rossman, M. G., & Kuhn, R. J. (2016). The 3.8 Å resolution cryo-EM structure of Zika virus. Science, 352(6284), 467-470.

14. Javed, F., Manzoor, K. N., Ali, M., Haq, I. U., Khan, A. A., Zaib, A., & Manzoor, S. (2018). Zika virus: what we need to know? Journal of basic microbiology, 58(1), 3-16.

15. Hamel, R., Dejarnac, O., Wichit, S., Ekchariyawat, P., Neyret, A., Luplertlop, N., ... & Missé, D. (2015). Biology of Zika virus infection in human skin cells. Journal of virology, 89(17), 8880-8896.

16. Weaver, S. C., Costa, F., Garcia-Blanco, M. A., Ko, A. I., Ribeiro, G. S., Saade, G., ... & Vasilakis, N. (2016). Zika virus: History, emergence, biology, and prospects for control. Antiviral research, 130, 69-80.
17. Pettersen, E. F., Goddard, T. D., Huang, C. C., Couch, G. S., Greenblatt, D. M., Meng, E. C., & Ferrin, T. E. (2004). UCSF Chimera—a visualization system for exploratory research and analysis. Journal of computational chemistry, 25(13), 1605-1612.
18. Lopez-Hernandez, A. E., Xie, Y., Guo, W., & Li, L. (2021). The electrostatic features of dengue virus capsid assembly. Journal of Computational Biophysics and Chemistry, 20(02), 201-207.
19. Li, L., Li, C., Sarkar, S., Zhang, J., Witham, S., Zhang, Z., ... & Alexov, E. (2012). DelPhi: a comprehensive suite for DelPhi software and associated resources. BMC biophysics, 5, 1-11.
20. Li, L., Chakravorty, A., & Alexov, E. (2017). DelPhiForce, a tool for electrostatic force calculations: Applications to macromolecular binding. Journal of computational chemistry, 38(9), 584-593.
21. Baker, N. A. (2005). Improving implicit solvent simulations: a Poisson-centric view. Current opinion in structural biology, 15(2), 137-143.
22. Dolinsky, T. J., Nielsen, J. E., McCammon, J. A., & Baker, N. A. (2004). PDB2PQR: an automated pipeline for the setup of Poisson–Boltzmann electrostatics calculations. Nucleic acids research, 32(suppl_2), W665-W667.
23. Humphrey, W., Dalke, A., & Schulten, K. (1996). VMD: visual molecular dynamics. Journal of molecular graphics, 14(1), 33-38.

24. Xian, Y., Xie, Y., Silva, S. M., Karki, C. B., Qiu, W., & Li, L. (2021). StructureMan: A structure manipulation tool to study large scale biomolecular interactions. Frontiers in molecular biosciences, 7, 627087.
25. Li, C., Jia, Z., Chakravorty, A., Pahari, S., Peng, Y., Basu, S., ... & Alexov, E. (2019). DelPhi suite: new developments and review of functionalities. Journal of computational chemistry, 40(28), 2502-2508.
26. Chakravorty, A., Jia, Z., Li, L., & Alexov, E. (2017). A new DelPhi feature for modeling electrostatic potential around proteins: Role of bound ions and implications for zeta-potential. Langmuir, 33(9), 2283-2295.
27. Guo, Wenhan, "Utilizing Computational Methods To Study The Biomolecules" (2022). Open Access Theses & Dissertations. 3610.
28. Xu, D., Tsai, C. J., & Nussinov, R. (1997). Hydrogen bonds and salt bridges across protein-protein interfaces. Protein engineering, 10(9), 999-1012.
29. Sindelar, Charles V., Zachary S. Hendsch, and Bruce Tidor. "Effects of salt bridges on protein structure and design." Protein Science 7.9 (1998): 1898-1914.
30. Phillips, J. C., Braun, R., Wang, W., Gumbart, J., Tajkhorshid, E., Villa, E., Chipot, C., Skeel, R. D., Kalé, L., & Schulten, K. (2005). Scalable molecular dynamics with NAMD. Journal of computational chemistry, 26(16), 1781–1802. https://doi.org/10.1002/jcc.20289

Vita

Cassandra Guadalupe Del Rio De Avila earned a Bachelor's degree in Physics from the Autonomous University of Zacatecas (UAZ) in Mexico in 2020. She enrolled at the University of Texas at El Paso (UTEP) in 2021 and is currently working towards a Master's degree in Physics at UTEP. During her undergraduate studies, she developed an interest in Biophysics and engaged in related projects. When she started her graduate studies, she chose to specialize in this field and became a member of the Computational Biophysics group under the supervision of Dr. Lin Li. Throughout her academic journey, Cassandra has participated in conferences, research summers, workshops, and scientific outreach events. Cassandra's passion for science has motivated her to pursue a Ph.D. program to deepen her knowledge and apply her Physics skills. After completing her Master's degree, she will begin her Ph.D. studies in the Biophysics program at the University of Wisconsin-Madison in the fall of 2023.

Contact: cgdelriode@miners.utep.edu